Research

CrossMark
click for updates

Author for correspondence:
V. Olden
e-mail: Vigdis.Olden@sintef.no

A review of cohesive zone modelling as an approach for numerically assessing hydrogen embrittlement of steel structures

L. Jemblie[1], V. Olden[2] and O. M. Akselsen[1,2]

[1]Department of Engineering Design and Materials, NTNU, 7456 Trondheim, Norway
[2]SINTEF Materials and Chemistry, 7456 Trondheim, Norway

Simulation of hydrogen embrittlement requires a coupled approach; on one side, the models describing hydrogen transport must account for local mechanical fields, while on the other side, the effect of hydrogen on the accelerated material damage must be implemented into the model describing crack initiation and growth. The present study presents a review of coupled diffusion and cohesive zone modelling as a method for numerically assessing hydrogen embrittlement of a steel structure. While the model is able to reproduce single experimental results by appropriate fitting of the cohesive parameters, there appears to be limitations in transferring these results to other hydrogen systems. Agreement may be improved by appropriately identifying the required input parameters for the particular system under study.

1. Introduction

Hydrogen induced degradation of mechanical properties, often termed hydrogen embrittlement (HE), is a well recognized threat for structural steels. It manifests as loss in ductility, strength and toughness, which may result in unexpected and premature catastrophic failures. The phenomenon was first reported by Johnson in 1874 [1], and has later been extensively researched both experimentally [2–7] and numerically [8–16], yielding a number of models accounting for the phenomenon.

THE ROYAL SOCIETY
PUBLISHING

However, no consensus about the basic mechanisms responsible for hydrogen embrittlement is reached yet. Two theories have advanced as the more accepted ones for the case of hydrogen degradation in steel: Hydrogen Enhanced Decohesion (HEDE), in which interstitial atomic hydrogen reduces the bond strength and thus the necessary energy to fracture [17,18]; and Hydrogen Enhanced Localized Plasticity (HELP), in which atomic hydrogen accelerates dislocation mobility through an elastic shielding effect which locally reduces the shear stress [19,20]. Today it is seemingly recognized that no single mechanism can comprehensively explain all the phenomena associated with hydrogen embrittlement. Rather it appears that different mechanisms apply to different systems, and that a combination of mechanisms is more likely in many cases.

In recent years, cohesive zone modelling (CZM) has gained increasing interest as suitable method for modelling hydrogen embrittlement [10–12,14,16], with the possibility of providing increased understanding of the involved process and their interactions combined with reduced time and costs compared to experimental programs. The damage process is classically described by interface elements, which constitutive relation is defined by a cohesive law (traction separation law). Simulation of hydrogen induced degradation requires a coupled approach, including modelling of transient mass transport, plastic deformation, fracture and their interactions. On one side, the models describing hydrogen diffusion must account for local mechanical field quantities; i.e. hydrostatic stress and plastic strain. On the other side, the effect of hydrogen on the accelerated material damage must be implemented into the cohesive law.

The present work reviews cohesive zone modelling as a method for numerically assessing the hydrogen embrittlement susceptibility of steel structures. Especially approaches for implementing hydrogen influence into the cohesive model and the coupling aspect between hydrogen transport and cohesive zone modelling is presented, followed by a discussion on some practical applications.

2. Hydrogen transport

To date, models of transient hydrogen diffusion generally account for trapping by dislocations and hydrostatic drift. Recent approaches include capturing the effect of multiple trap sites and hydrogen transport by dislocations [13,21,22]. An extensive review of hydrogen transport models is beyond the scope of this work, and only a short summery covering the most governing aspects is given. For a more thorough description, the reader is referred to Sofronis et al. [8,21,22] and Krom et al. [9].

(a) Trapping of hydrogen

Atomic hydrogen is generally considered to reside either at normal interstitial lattice sites (NILS) or being trapped at microstructural defects like dislocations, carbides, grain boundaries and interfaces. Given a metal lattice, the hydrogen concentration in NILS is given by [8]

$$C_L = \beta \theta_L N_L \tag{2.1}$$

where θ_L is the lattice site occupancy, N_L is the density of solvent atoms and β is the number of NILS per solvent atom. Similarly, the concentration of hydrogen trapped at a given site is [8]

$$C_T = \alpha \theta_T N_T \tag{2.2}$$

where θ_T is the occupancy, N_T is the density of the specific trap site (dislocation, carbide etc.) and α is the number of sites per trap. According to Oriani's theory [23], hydrogen in NILS and hydrogen in reversible trapping sites are always in local equilibrium, such that

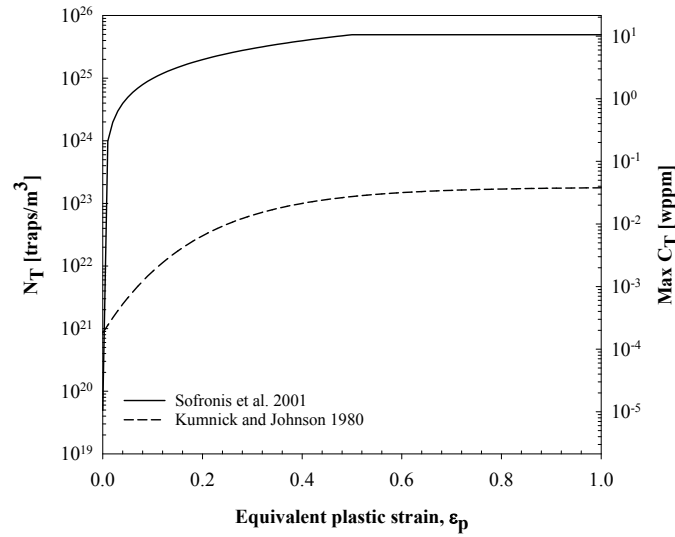$$\frac{\theta_T}{1 - \theta_T} = \frac{\theta_L}{1 - \theta_L} \exp\left(\frac{E_B}{RT}\right) \tag{2.3}$$

Figure 1. Dislocation trap densities according to the work by Kumnick and Johnson [2] and the model by Sofronis et al. [24,25]. In calculating C_T, it is assumed $\alpha\theta_T = 1$, which accordingly gives the maximum possible hydrogen concentration trapped at dislocations.

with E_B being the trap binding energy. This approach is valid in the domain of rapid trap filling and escape kinetics.

For microstructural defects like carbides and grain boundaries, the trap densities are often assumed constant throughout the material. For dislocations, however, the trap density varies point-wise dependent on the local plastic strain. Based on experimental work by Kumnick and Johnson [2] on hydrogen trapping in deformed iron, Sofronis and McMeeking [8] proposed the following relationship between the dislocation trap density and the equivalent plastic strain ε_p:

$$\log N_T^{(d)} = 23.26 - 2.33 \exp(-5.5\varepsilon_p) \tag{2.4}$$

An alternative theoretical approach has been proposed by Sofronis et al. [24,25], assuming one trap site per atomic plane threaded by a dislocation, maintaining that this is consistent with the experimental work of Thomas [26]. The dislocation trap density is then expressed as a function of the dislocation density ρ and the lattice parameter a

$$N_T^{(d)} = \sqrt{2}\frac{\rho}{a} \tag{2.5}$$

The dislocation density (measured in dislocation line length per cubic meter) is considered to vary linearly with the equivalent plastic strain according to

$$\rho = \begin{cases} \rho_0 + \gamma\varepsilon_p & \text{for } \varepsilon_p < 0.5 \\ 10^{16} & \text{for } \varepsilon_p \geq 0.5 \end{cases} \tag{2.6}$$

where $\rho_0 = 10^{10}$ line length/m^3, denotes the dislocation density at zero plastic strain, and $\gamma = 2.0 \cdot 10^{16}$ line length/m^3. Using the lattice parameter of BCC iron $a = 2.86$ Å, the trap densities according to the data from Kumnick and Johnson [2] and the model by Sofronis et al. [24,25] are compared in Figure 1. It can be concluded that the model by Sofronis et al. yields a dislocation trap density about three orders of magnitude larger than the data by Kumnick and Johnson.

(b) Hydrogen diffusion

The governing model for hydrogen transport, as developed by Sofronis and McMeeking [8], yields

$$\frac{\partial}{\partial t}(C_L + C_T) = -\nabla \mathbf{J} \tag{2.7}$$

where

$$\mathbf{J} = -D\left(\nabla C_L + \frac{C_L \overline{V}_H}{RT}\nabla p\right) \tag{2.8}$$

is the hydrogen flux of diffusion particles through NILS, motivated by chemical potential gradients. $\overline{V}_H$ is the partial molar volume of hydrogen and p is the hydrostatic pressure. Despite its small size, dissolved hydrogen atoms induces a distortion in the steel lattice, resulting in the formation of hydrostatic compressive stresses and volume dilatation [27]. The chemical potential of hydrogen is therefore lowered in regions of tensile hydrostatic stresses, and consequently a hydrogen flux is generated towards these regions. The opposite effect occurs on encountering compressive hydrostatic stresses. Substituting Equation (2.8) in (2.7), under the assumption of Oriani's theory of equilibrium [23], provides the governing model for transient hydrogen transport model, derived by Sofronis and McMeeking [8] and later modified by Krom et al. [9]:

$$\frac{C_L + C_T(1 - \theta_T)}{C_L}\frac{\partial C_L}{\partial t} = D\nabla^2 C_L + \nabla \cdot \left(\frac{D\overline{V}_H}{RT}C_L\nabla p\right) - \alpha\theta_T \frac{dN_T}{d\varepsilon_p}\frac{d\varepsilon_p}{dt} \tag{2.9}$$

This model accounts for trapping by dislocations and hydrostatic drift. The last term is the plastic strain rate factor, accounting for the effect of the strain rate on the transient hydrogen concentrations. It disappears in the absence of dislocation trap sites ($dN_T/d\varepsilon_p = 0$).

3. A CZM approach to hydrogen embrittlement

Cohesive models were first formulated by Barenblatt [28] and Dugdale [29], who introduced finite non-linear cohesive tractions in front of an existing crack, as a mean to overcome the crack tip stress singularity. To date, the cohesive model is extensively applied for crack propagation analysis using the finite element method. Among the various approaches available, it is appealing in that it requires few parameters and in its universality of applicability [30].

(a) The cohesive model

The cohesive theory of fracture is a purely phenomenological continuum framework, not representative of any physical material. The constitutive response of the material is divided in two parts; an arbitrary material law relating the stresses and strains in the bulk regions adjacent to the crack faces, and a cohesive law characterizing the separation process by describing the forces opposing crack formation (tractions) as a function of the incipient crack surfaces' separation distance. Common to most cohesive laws is that they can be described by two independent parameters out of the following three: the cohesive strength σ_C, the critical separation δ_C and the cohesive energy Γ_C. Figure 2 displays three commonly applied cohesive laws, plotted as normalized traction versus separation; a linear decreasing law suggested for brittle materials by Hillerborg et al. [31], a polynomial law suggested by Needleman [32] for ductile materials and, more recently, a versatile trapezoidal law suggested by Scheider [33] also for ductile materials. The area embedded by the curve represents the cohesive energy. A more thorough compilation of cohesive laws can be found in literature, e.g. Shet and Chandra [34] or Brocks et al. [35].

An intrinsic disconnection exists between atomistic and engineering cohesive descriptions, where the fundamental formulation by Barenblatt [28] is equivalent to the atomistic conception of the cohesive zone. Typically, the work of separation differs by orders of magnitude, suggesting the engineering description contains elements of the plastic work of fracture. In cohesive zone modelling, the cohesive energy can physically be understood as the total energy dissipated by the cohesive element during separation.
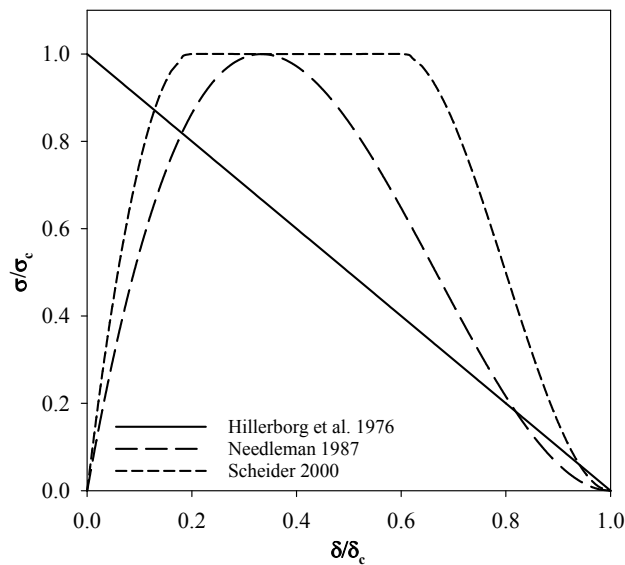
Figure 2. Cohesive laws by Hillerborg et al. [31], Needleman [32] and Scheider [33].

The influence of the shape of the cohesive law on the results is controversial; while Scheider and Brocks [36] found significant effect on their calculated results, Tvergaard and Hutchinson [37] concluded that such an influence is negligible. Irrespectively, the cohesive law has to be chosen in relation to the actual micromechanical damage mechanism leading to failure. Values of the cohesive parameters should be chosen so that they do not affect the overall compliance of the system [15]. Alvaro et al. [15] points out the importance of this in relation to modelling hydrogen embrittlement. A choice of cohesive parameters which infers low values of the initial stiffness will results in lower values of hydrostatic stress and equivalent plastic strain, consequently affecting the lattice and trapped hydrogen populations.

Despite cohesive zone simulation being straightforward, it has limitations when it comes to modelling crack nucleation, failing to produce a converged solution at the point were the crack first nucleates. These problems, which are especially prominent in performing a coupled hydrogen transport and cohesive analysis, are attributed to a snap-back instability that occurs just after the stress reaches the peak strength of the interface [38]. Gao and Bower [38] found that adding a small viscosity term in the cohesive relation significantly increases the numerical stability. Yu et al. [39] have applied the viscosity term by Gao and Bower [38] in a three step, un-coupled, hydrogen informed cohesive zone model under constant displacement, and found the viscous regularization to be effective in solving the convergence problem with good accuracy. In relation to performing a coupled hydrogen transport and cohesive analysis, it is still some uncertainty as to whether a model containing this viscosity term is able to accurately predict the time to fracture.

(b) Implementing hydrogen influence

Most known attempts of implementing hydrogen influence into the cohesive model is through the HEDE principle [11,15,16,40–42]; hydrogen reduction of the cohesive energy at fracture. In its most simplistic approach, the critical hydrogen dependent cohesive stress $\sigma_C(C)$ is assumed to
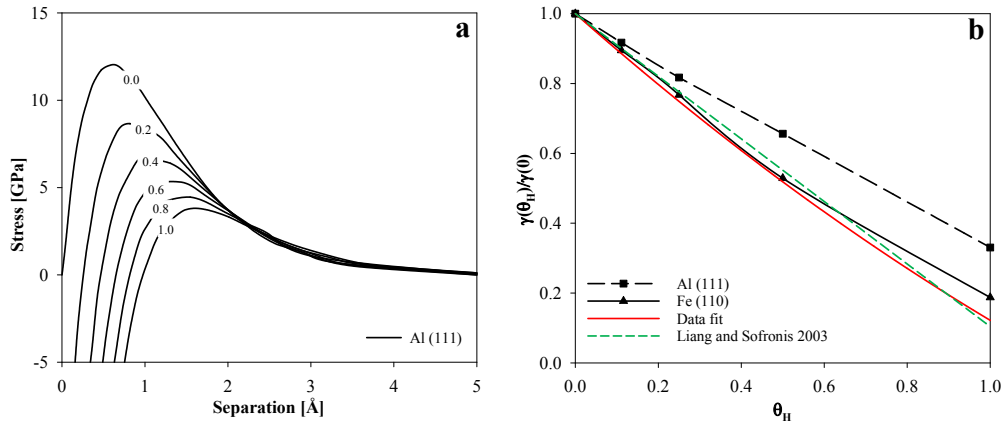
Figure 3. Hydrogen effect on decohesion by quantum-mechanical approaches: (a) Traction separation curves for decohesion along Al(111) planes with a hydrogen coverage between 0 and 1, by Van der Ven and Ceder [45]. (b) Cleavage energy for decohesion along Al(111) and Fe(110) as a function of hydrogen coverage, by Jiang and Carter [46].

decrease linearly with increasing hydrogen concentration

$$\sigma_C(C) = \sigma_C(0)(1 - \xi C) \tag{3.1}$$

where $\sigma_C(0)$ is the critical cohesive stress with no hydrogen influence and ξ is a softening parameter, often found by fitting to experimental results [42–44]. This formulation predicts a hydrogen influenced fracture toughness $K_{IC} = 0$ and, thus, complete decohesion upon the attainment of a certain critical hydrogen concentration.

In recent years, quantum-mechanical approaches by first principle calculations have been increasingly used to quantify the effect of hydrogen on decohesion [45,46]. A key factor is that hydrogen strongly prefers to stay on the surface compared to in the bulk, which provides a driving force for decohesion and, thereby, embrittlement. Using an equilibrium thermodynamic description, Van der Ven and Ceder [45] have obtained a complete set of traction-separation curves for decohesion along Al(111) planes with a hydrogen coverage between 0 and 1 (1 representing the saturation value). The results are displayed in Figure 3a, revealing a decrease in the cohesive energy with increasing hydrogen coverage. The critical separation, however, was found to be insensitive to hydrogen throughout the given range.

Jiang and Carter [46] have calculated the ideal cleavage energy (equal to twice the surface energy, γ) of Fe and Al in the presence of various amounts of hydrogen within the framework of a Born-Haber thermodynamic cycle. The main idea is that hydrogen dissolved in metals quickly segregate to the incipient crack surfaces as a crack begins to form. An almost linear decrease in cleavage energy with increasing hydrogen coverage is observed for both Al(111) and Fe(110), as displayed in Figure 3b. A fit to the data for the H/Fe system yields [11]

$$\frac{\gamma(\theta_H)}{\gamma(0)} = 1 - 1.0467\theta_H + 0.1687\theta_H^2 \tag{3.2}$$

where θ_H is the surface hydrogen coverage, $\gamma(\theta_H)$ is the hydrogen dependent surface energy and $\gamma(0)$ is the surface energy with no hydrogen influence. The data fit is illustrated by the red line in Figure 3b. The definition of hydrogen coverage follows the Langmuir-McLean isotherm [47], relating it to the bulk hydrogen concentration C (unit mol H/mol Fe) through

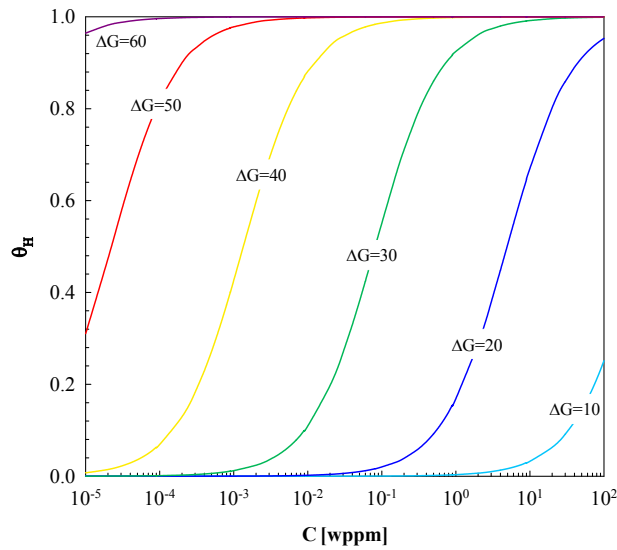$$\theta_H = \frac{C}{C + \exp(-\Delta G_b^0/RT)} \tag{3.3}$$

Figure 4. Hydrogen coverage as a function of hydrogen concentration, for various levels of Gibbs energy (kJ/mol). Plotted according to the Langmuir-McLean isotherm [47].

where ΔG_b^0 is the Gibbs energy difference between surface and bulk material, surface being any microstructural interface like crystallographic plane, grain boundary etc. The hydrogen coverage as a function of hydrogen concentration is plotted in Figure 4 for various levels of Gibbs energy ranging between 10 kJ/mol and 60 kJ/mol. It is evident that a given value of Gibbs energy covers a concentration range of about 4 orders of magnitude, where the lower bound represents a hydrogen concentration threshold for embrittlement and the upper bound represents a corresponding saturation level.

Extrapolation of nanometre scale quantum mechanical calculations to macroscopic scale continuum models entails some difficulty. Atomistic predictions of peak stresses are on the order of the theoretical strength of the crystal, while opening displacements are only a few angstroms [11,48,49]. Further, the cohesive zone sizes attendant to first principle calculations are on the nanometre scale, making finite element calculations unfeasible, as the mesh must fully resolve the cohesive zone in order to obtain a converged solution. Using a renormalization procedure described by Nguyen and Ortiz [48] and Hayes et al. [49] to scale the atomic-level cohesive properties up to the continuum scale, Serebrinsky et al. [11] have developed a cohesive model of fracture, accounting for the effect of hydrogen segregation by a quantum-mechanical treatment. Based on the relation in Equation (3.2), the following coupling between hydrogen coverage and the critical hydrogen dependent cohesive stress $\sigma_C(\theta_H)$ is suggested for bcc iron [11]

$$\frac{\sigma_C(\theta_H)}{\sigma_C(0)} = 1 - 1.0467\theta_H + 0.1687\theta_H^2 \tag{3.4}$$

The critical separation δ_C is deemed constant, insensitive to the hydrogen coverage, based on the results from Van der Ven and Ceder [45] in Figure 3a. The influence of hydrogen, in terms of hydrogen coverage, on the cohesive strength and consequently on the cohesive energy is illustrated in Figure 5a for the polynomial cohesive law by Needleman [32]. Using the coupling between hydrogen coverage and bulk concentration as supplied by the Langmuir-McLean isotherm, Serebrinsky et al. [11] suggested $\Delta G_b^0 = 30$ kJ/mol, which represents the trapping energy of hydrogen at a Fe grain boundary, yielding a threshold concentration of about 0.001 wppm and an embrittlement saturation level of about 5 wppm. Hence, a concentration level close
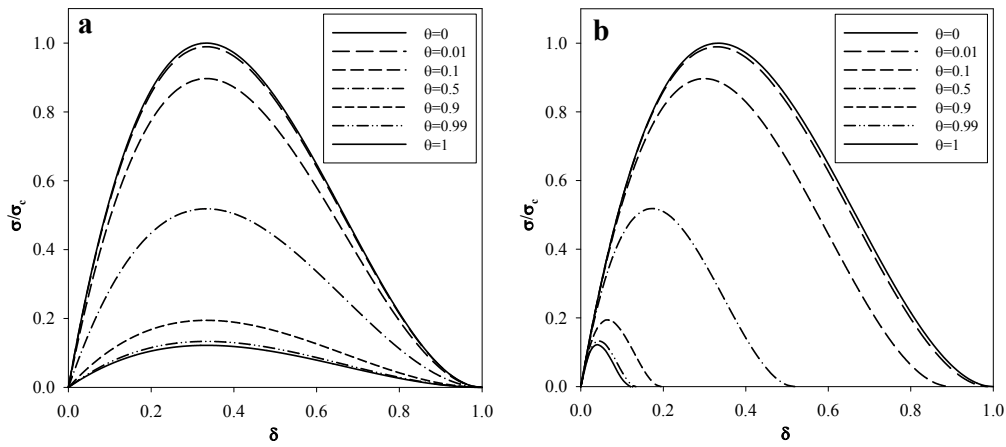
Figure 5. Reduction in cohesive energy at different levels of hydrogen coverage for the polynomial cohesive law by Needleman [32], where (a) illustrates hydrogen influence on the cohesive strength only (single) and (b) illustrates hydrogen influence on both the cohesive strength and the critical separation (double).

to the theoretical solubility of hydrogen in iron (about 10^{-4} wppm [50]) should not induce any effect on the cohesive properties, implying the importance of trapped hydrogen.

Raykar et al. [42] have proposed a hydrogen damaging effect both on the cohesive strength and on the critical separation, basing this choice on the experimentally observed reduction in both ultimate tensile strength and percentage elongation in the presence of hydrogen. A linear dependence on hydrogen concentration according to Equation (3.1) was chosen for both parameters. The same approach has also been applied by Gobbi et al. [51], however here with a hydrogen dependence according to the work by Serebrinsky et al. [11]. Figure 5b illustrates hydrogen influence, in terms of hydrogen coverage, according to Equation (3.4), on both the cohesive strength and on the critical separation, for the polynomial cohesive law by Needleman [32]. A comparison of the effect of single and double hydrogen influence on the critical cohesive energy at fracture is made in Figure 6, where the cohesive energy is plotted as a function of the hydrogen coverage for the two cases in Figure 5, displaying an enhanced hydrogen damaging effect with double hydrogen influence. Although this approach was found to display a reasonable fit with experimental data [42,51], no quantification of any effect of hydrogen on the critical separation is found to date.

Liang and Sofronis [10] have proposed an alternative model for hydrogen decohesion, based on work by, amongst others, Rice and Wang [52,53], who estimated the effect of segregated hydrogen on interface cohesion from a general thermodynamic framework. The resulting hydrogen dependent cohesive strength is expressed for two limiting cases of interfacial separation: separation at constant hydrogen concentration (denoted fast separation) given by Equation (3.5), and separation at constant hydrogen chemical potential (denoted slow separation) given by Equation (3.6)

$$\sigma_C(\Gamma) = \sigma_C(0) \left(1 - \frac{\Gamma_{\max}(\Delta g_i^0 - \Delta g_s^0)}{(2\gamma_{\mathrm{int}})_0} \frac{\Gamma}{\Gamma_{\max}} \right) \tag{3.5}$$

$$\sigma_C(\mu) = \sigma_C(0) \left(1 - \frac{RT\Gamma_{\max}}{(2\gamma_{\mathrm{int}})_0} \ln \left(\frac{1 + (m-1)(\Gamma_0/\Gamma_{\max})^2}{1 - (\Gamma_0/\Gamma_{\max})} \right) \right) \tag{3.6}$$

Δg_i^0 and Δg_s^0 are the Gibbs energy of segregation for the interface and free surface, respectively, $\Gamma/\Gamma_{\max}$ is the interfacial hydrogen coverage and $m = \exp((\Delta g_i^0 - \Delta g_s^0)/RT)$. The proposed model was used to simulate separation along a chromium carbide/fcc matrix (nickel alloy
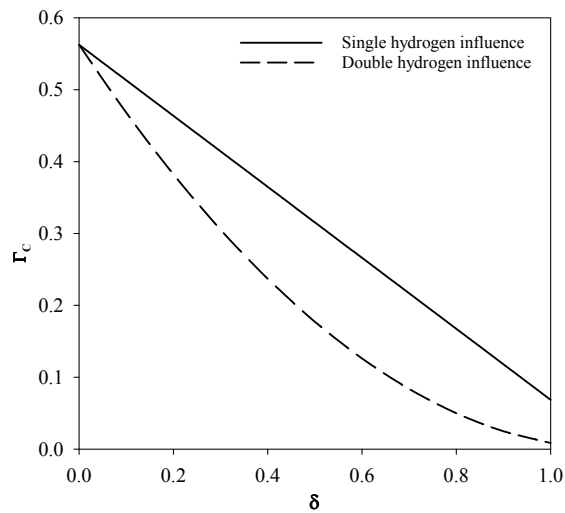
Figure 6. Relationship between critical cohesive energy at fracture and hydrogen coverage for the polynomial cohesive law by Needleman [32]. Single hydrogen influence denotes hydrogen reduction of the critical cohesive stress. Double hydrogen influence denotes hydrogen reduction of the critical cohesive stress and of the critical separation.
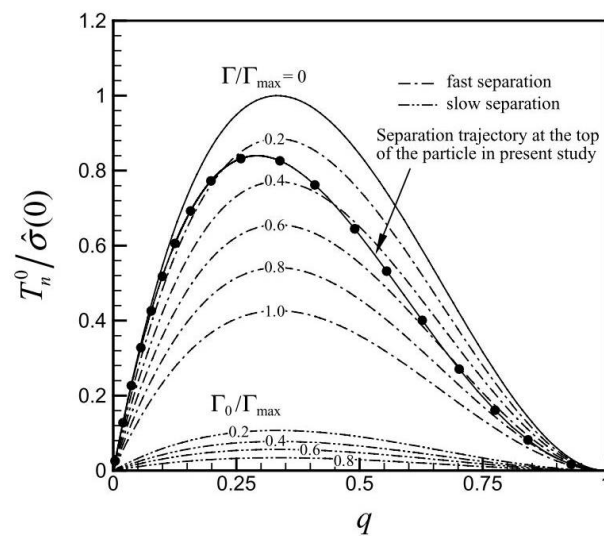

Figure 7. Hydrogen influenced cohesive laws from the decohesion model by Liang and Sofronis [10], T_n^0 is the normal traction and q is a non-dimensional separation parameter.

690) interface. The resulting range of polynomial cohesive laws (Needleman [32]) for various interfacial hydrogen coverage values is presented in Figure 7. Using parameters representing of Fe (110); $(2\gamma_{\text{int}})_0 = 4.86$ J/m^2 and $\Gamma_{\text{max}} = 5.85 \cdot 10^{-5}$ mol/m^2 [46], assuming $\Delta g_i^0 - \Delta g_s^0 = 74.5$ kJ/mol [13], the hydrogen dependent cohesive stress for the fast separation case can be estimated. The result is plotted as the green dotted line in Figure 3b, representing a good fit with the result by Jiang and Carter.
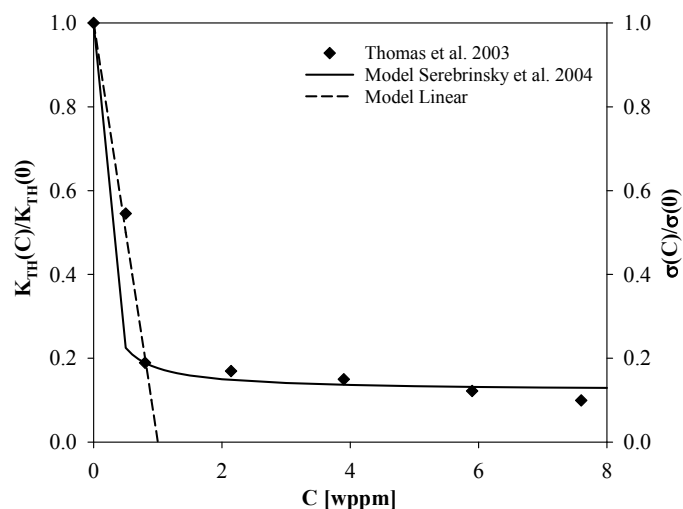
Figure 8. Normalized threshold stress intensity factor and normalized hydrogen dependent cohesive stress as a function of hydrogen concentration, according to experimental data by Thomas et al. [4], the linear decohesion model and the exponential decohesion model by Serebrinsky et al. [11], with $\Delta G_b^0 = 30$ kJ/mol.

(c) Coupling of diffusion and mechanical models

The Langmuir-McLean isotherm defines the necessary coupling between the hydrogen diffusion model in Section 2 and the hydrogen-dependent cohesive law described in the previous section. The coupling takes place in two ways: first, hydrogen accelerates material damage by building up over the cohesive zone, as indicated by Equation (3.3) and (3.4). Second, hydrogen transport is influenced by the local hydrostatic stress and plastic strain fields, according to Equation (2.9).

Experimental results investigating the effect of hydrogen on fracture generally displays a weaker effect of hydrogen with increasing concentration [4,6,13]. Thomas et al. [4] found that the threshold stress intensity factor for hydrogen embrittlement in AERMET 100 steel decreased sharply with an increasing diffusible hydrogen concentration up to 2 wppm, and more modestly with higher concentrations. The result is displayed in Figure 8 for a normalized threshold stress intensity factor, together with the normalized hydrogen dependent cohesive stress according to the linear model in Equation (3.1) and the model by Serebrinsky et al. [11], with the hydrogen concentration calculated according to the Langmuir-McLean isotherm for $\Delta G_b^0 = 30$ kJ/mol. The model by Serebrinsky et al. [11] captures the exponential embrittlement effect of hydrogen, attaining a saturation level at high concentrations. The linear model, fitted to the initial part of the experimental data, gives a reasonable approximation at low concentrations only. The results confirms the necessity of a saturating hydrogen embrittlement law, as also pointed out by Serebrinsky et al. [11].

4. Practical applications of the coupled cohesive model

The capability of the model to trustfully predict hydrogen induced crack nucleation and propagation in structural steel applications is of key importance for further developments. An engineering tool, able to partly replace time consuming and costly experimental programs, should be of general validity and provide robustness and transferability to other material systems and environments. While most studies are able to reproduce single experimental results by appropriate fitting to the cohesive parameters, there still appears to be limitations on transferring
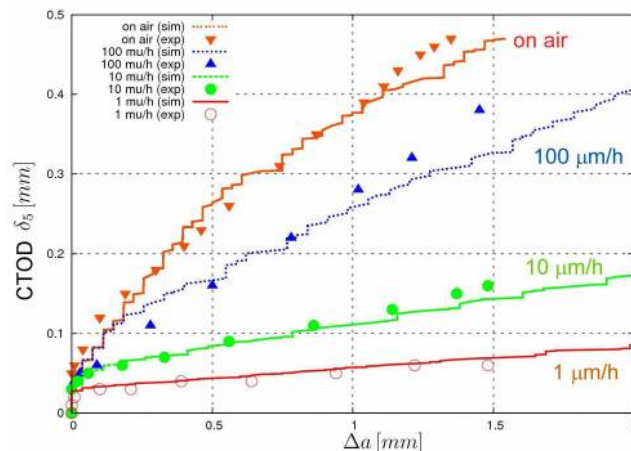
Figure 9. CTOD-R curves for various deformation rates, comparing experimental tests (symbol) and simulation results (lines). From Brocks et al. [14].

these results to other hydrogen systems [15,16]. Moriconi et al. [16] have developed a cohesive model based on coupled effects between mechanical cyclic loading and hydrogen diffusion. Simulated fatigue crack growth was compared with experimental measurements on martensitic stainless steel under gaseous hydrogen. The results indicate that while the model was able to reasonably predict the fatigue crack growth behaviour under low hydrogen pressure, it failed to account for the enhanced crack growth observed at high pressures. Limitations in the model, particular in the case of lattice diffusion, were pointed out as possible explanations, however no conclusion were drawn.

Recently, Dadfarnia et al. [22] have extended the hydrogen transport model by Sofronis and McMeeking [8] and Krom et al. [9] (Equation (2.9)) to account for hydrogen transport by dislocations. Moving dislocations represent moving traps that carry hydrogen atoms. Thus, hydrogen is transported by both diffusion through NILS and by mobile dislocations. Results from numerical simulations indicate that dislocation transport can contribute to an elevation of the local hydrogen concentration above levels predicted by the classical diffusion model, with the effect being larger for materials with lower hydrogen diffusion coefficient and higher dislocation trap binding energy.

Brocks et al. [14,54] have developed a model of hydrogen induced cracking, which in addition to the coupled interactions of hydrogen diffusion and reduced cohesive strength, also includes the effect of surface kinetics on hydrogen absorption and hydrogen induced softening of the local yield strength (HELP mechanism). A thorough description of the model can be found in [14,54]. By including both local hydrogen softening and hydrogen induced lowering of the local cohesive strength, the model describes an attempt in the direction of including both the HEDE and the HELP degradation mechanisms and their interactions. Simulated CTOD-R curves were compared with experimental results on high strength low alloy structural steel, with appropriate fitting of the cohesive parameters and their dependence on the lattice hydrogen concentration. The results are displayed in Figure 9 for various deformation rates, where the two mid curves (10 μm h^{-1} and 100 μm h^{-1}) represent real predictions, capturing the rate dependence of the R-curves due to hydrogen diffusion quite well. While numerous experimental measurements are necessary in order to determine the required input parameters, the authors argue the model may, to some extent, replace expensive laboratory testing, especially considering its transferability to other systems by identifying the required parameters.
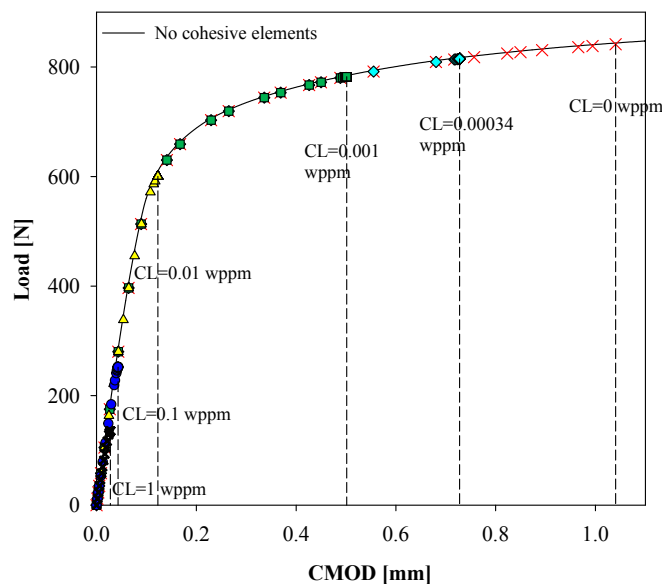
Figure 10. Load-CMOD curves according to coupled hydrogen diffusion and cohesive simulations of a bi-metallic compact tension specimen, comparing various initial lattice hydrogen concentrations. The vertical lines indicate points of fracture for the respective concentration levels.

Recent work by the present authors includes coupled hydrogen diffusion and cohesive zone simulations, with the aim of reproducing fracture mechanical tests of bi-metallic compact tension specimens performed in air and under cathodic protection (3.5 % NaCl solution at -1050 mV$_{SCE}$). The developed model is based on the presented work by Serebrinsky et al. [11], with $\Delta G_b^0 = 30$ kJ/mol. A best fit of the cohesive parameters to the experimental results in air was achieved for $\sigma_C = 1188$ MPa ($3.5\sigma_y$) and $\delta_C = 0.005$ mm. Taking into account the effect of hydrogen on the critical cohesive stress, the initial lattice hydrogen concentration was varied from 0.00034 wppm to 1 wppm, corresponding to the theoretical solubility of hydrogen in ferrite [50] and a 3 % NaCl [11,55] aqueous solution, respectively. The resulting load-CMOD curves for various hydrogen concentrations are displayed in Figure 10, where the dotted, vertical lines indicate the points of fracture for the respective concentration. The corresponding traction vs separation curves are compared in Figure 11. Fracture is defined as the encountering of divergence, just after the stress reaches the peak strength of the interface.

The model is clearly able to account for a decrease in the fracture toughness with increasing hydrogen concentration, while also maintaining the stiffness of the cohesive element. It fails, however, to provide a solution comparable with experimentally measured hydrogen concentrations. For experimental testing under cathodic protection, failure is observed at a CMOD value of approximately 0.3 mm, which according to Figure 10 would indicate a lattice hydrogen concentration in the range 0.001-0.01 wppm. This is 2-3 orders of magnitude below the measured concentration of 1.5-2.5 wppm [55]. Serebrinsky et al. [11] suggested that agreement for high hydrogen concentrations might be improved by considering different adsorption sites at the cracking interface, with a distribution of adsorption energies. Novak et al. [13] reported that high-binding energy traps cannot account for the loss in strength observed on hydrogen charged steel, because these traps remain saturated with hydrogen regardless of loading conditions and/or hydrogen exposure conditions. Thus, lowering the ΔG_b^0 level could be justified, identifying parameters according to the particular system in question.
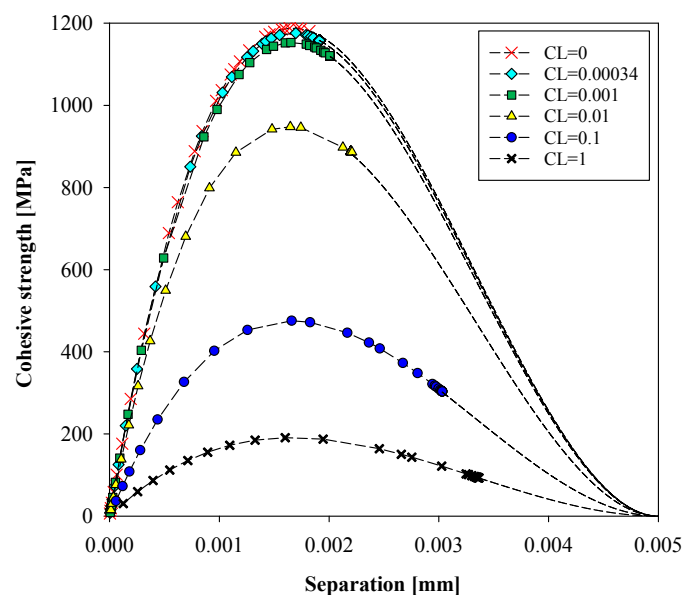
Figure 11. Comparing traction vs separation curves for various initial lattice hydrogen concentrations.

5. Conclusion

A coupled mass transport and cohesive zone modelling approach for simulating hydrogen induced cracking is described and discussed. To date, cohesive zone modelling approaches have proven to be able to reproduce single experimental results by appropriate fitting of the cohesive parameters. However, there appears to be limitations in transferring these results to other hydrogen systems. Agreement may be improved by appropriately identifying the required input parameters for the particular system under study.

Authors' Contributions. All authors have contributed to this review article.

References

1. W. H. Johnson.
   On some remarkable changes produced in iron and steel by the action of hydrogen and acids.
   Proc. R. Soc. London, 23:168–179, 1874.
2. A. J. Kumnick and H. H. Johnson.
   Deep trapping states for hydrogen in deformed iron.
   Acta Metall., 28(1):33–39, 1980.
   doi: 10.1016/0001-6160(80)90038-3.
3. W. Y. Choo and J. Lee.
   Thermal analysis of trapped hydrogen in pure iron.
   Metall. Trans. A, 13(1):135–140, 1982.
   doi: 10.1007/BF02642424.
4. Richard L. S. Thomas, John R. Scully, and Richard P. Gangloff.

Internal hydrogen embrittlement of ultrahigh-strength AERMET 100 steel.
Metall. Mater. Trans. A, 34(2):327–344, 2003.
doi: 10.1007/s11661-003-0334-3.

5. D. Li, R. P. Gangloff, and J. R. Scully.
Hydrogen trap states in ultrahigh-strength AERMET 100 steel.
Metall. Mater. Trans. A, 35(3):849–864, 2004.
doi: 10.1007/s11661-004-0011-1.

6. T. Zakroczymski, A. Glowacka, and W. Swiatnicki.
Effect of hydrogen concentration on the embrittlement of a duplex stainless steel.
Corros. Sci., 47(6):1403–1414, 2005.
doi: 10.1016/j.corsci.2004.07.036.

7. A. Alvaro, V. Olden, A. Macadre, and Odd Magne Akselsen.
Hydrogen embrittlement susceptibility of a weld simulated X70 heat affected zone under H2 pressure.
Mater. Sci. Eng. A, 597:29–36, 2014.
doi: 10.1016/j.msea.2013.12.042.

8. P. Sofronis and R.M. McMeeking.
Numerical analysis of hydrogen transport near a blunting crack tip.
J. Mech. Phys. Solids, 37(3):317–350, 1989.
doi: 10.1016/0022-5096(89)90002-1.

9. A. H. M. Krom, R. W. J. Koers, and A. Bakker.
Hydrogen transport near a blunting crack tip.
J. Mech. Phys. Solids, 47(4):971–992, 1999.
doi: 10.1016/S0022-5096(98)00064-7.

10. Y. Liang and P. Sofronis.
Toward a phenomenological description of hydrogen-induced decohesion at particle/matrix interfaces.
J. Mech. Phys. Solids, 51(8):1509–1531, 2003.
doi: 10.1016/S0022-5096(03)00052-8.

11. A. Serebrinsky, E. A. Carter, and M. Ortiz.
A quantum-mechanically informed continuum model of hydrogen embrittlement.
J. Mech. Phys. Solids, 52:2403–2430, 2004.
doi: 10.1016/j.jmps.2004.02.010.

12. V. Olden, C. Thaulow, R. Johnsen, E. Østby, and T. Berstad.
Influence of hydrogen from cathodic protection on the fracture susceptibility of 25%Cr duplex stainless steel-Constant load SENT testing and FE-modelling using hydrogen influenced cohesive zone elements.
Eng. Fract. Mech., 76(7):827–844, 2009.
doi: 10.1016/j.engfracmech.2008.11.011.

13. P. Novak, R. Yuan, B. P. Somerday, P. Sofronis, and R. O. Ritchie.
A statistical, physical-based, micro-mechanical model of hydrogen-induced intergranular fracture in steel.
J. Mech. Phys. Solids, 58(2):206–226, 2010.
doi: 10.1016/j.jmps.2009.10.005.

14. W. Brocks, R. Falkenberg, and I. Scheider.
Coupling aspects in the simulation of hydrogen-induced stress-corrosion cracking.
Procedia IUTAM, 3:11–24, 2012.
doi: 10.1016/j.piutam.2012.03.002.

15. A. Alvaro, V. Olden, and O. M. Akselsen.
3D cohesive modelling of hydrogen embrittlement in the heat affected zone of an X70 pipeline steel - Part II.
Int. J. Hydrogen Energy, 39:3528–3541, 2014.
doi: 10.1016/j.ijhydene.2013.12.097.

16. C. Moriconi, G. Hénaff, and D. Halm.
Cohesive zone modeling of fatigue crack propagation assisted by gaseous hydrogen in metals.
Int. J. Fatigue, 68:56–66, 2014.
doi: 10.1016/j.ijfatigue.2014.06.007.

17. A. R. Troiano.

The role of hydrogen and other interstitials in the mechanical behaviour of metals.
Trans. ASM, 52:54–80, 1960.

18. R. A. Oriani.
A mechanistic theory of hydrogen embrittlement of steels.
Berichte der Bunsengesellschaft für Phys. Chemie, 76(8):848–857, 1972.
doi: 10.1002/bbpc.19720760864.

19. H. K. Birnbaum and P. Sofronis.
Hydrogen-enhanced localized plasticity-a mechanism for hydrogen-related fracture.
Mater. Sci. Eng. A, 176(1-2):191–202, 1994.
doi: 10.1016/0921-5093(94)90975-X.

20. I. M. Robertson, H. K. Birnbaum, and P. Sofronis.
Chapter 91 Hydrogen Effects on Plasticity.
Dislocations in Solids, 15(09):249–293, 2009.
doi: 10.1016/S1572-4859(09)01504-6.

21. M. Dadfarnia, P. Sofronis, and T. Neeraj.
Hydrogen interaction with multiple traps: Can it be used to mitigate embrittlement?
Int. J. Hydrogen Energy, 36(16):10141–10148, 2011.
doi: 10.1016/j.ijhydene.2011.05.027.

22. M. Dadfarnia, M. L. Martin, A. Nagao, P. Sofronis, and I. M. Robertson.
Modeling hydrogen transport by dislocations.
J. Mech. Phys. Solids, 78:511–525, 2015.
doi: 10.1016/j.jmps.2015.03.002.

23. R A Oriani.
The diffusion and trapping of hydrogen in steel.
Acta Metall., 18(1):147–157, 1970.

24. P. Sofronis, Y. Liang, and N. Aravas.
Hydrogen induced shear localization of the plastic flow in metals and alloys.
Eur. J. Mech. A - Solids, 20:857–872, 2001.
doi: 10.1016/S0997-7538(01)01179-2.

25. J. Lufrano, P. Sofronis, and D. Symons.
Hydrogen transport and large strain elastoplasticity near a notch in alloy X-750.
Eng. Fract. Mech., 59(6):827–845, 1998.
doi: 10.1016/S0013-7944(97)00142-2.

26. G. J. Thomas.
Hydrogen trapping in FCC metals.
In I. M. Bernstein and A. W. Thompson, editors, *Hydrog. Eff. Mater.*, pages 77–85. Transactions of the Metallurgical Society of AIME, 1980.

27. J. P. Chateau, D. Delafosse, and T. Magnin.
Numerical simulations of hydrogen-dislocation interactions in fcc stainless steels.: part I: hydrogen-islocation interactions in bulk crystals.
Acta Mater., 50(6):1507–1522, 2002.
doi: 10.1016/S1359-6454(02)00008-3.

28. G. I. Barenblatt.
The mathematical theory of equilibrium cracks in brittle fracture.
Adv. Appl. Mech., 7:55–129, 1962.

29. D. S. Dugdale.
Yielding of steel sheets containing slits.
J. Mech. Phys. Solids, 8:100–104, 1960.

30. A. Cornec, I. Scheider, and K. H. Schwalbe.
On the practical application of the cohesive model.
Eng. Fract. Mech., 70:1963–1987, 2003.
doi: 10.1016/S0013-7944(03)00134-6.

31. A. Hillerborg, M. Modéer, and P.-E. Petersson.
Analysis of crack formation and crack growth in concrete by means of fracture mechanics and finite elements.
Cem. Concr. Res., 6(6):773–781, 1976.
doi: 10.1016/0008-8846(76)90007-7.

32. A. Needleman.

A continuum model for void nucleation by inclusion debonding.
J. Appl. Mech., 54(3):525–531, 1987.
doi: 10.1115/1.3173064.

33. I. Scheider.
Simulation of cup-cone fracture in round bars using the cohesive zone model.
In *First MIT Conf. Comput. Fluid Solid Mech.*, pages 460–462. Elsevier, 2001.

34. C. Shet and N. Chandra.
Analysis of energy balance when using cohesive zone models to simulate fracture processes.
J. Eng. Mater. Technol. Asme, 124(4):440–450, 2002.
doi: 10.1115/1.1494093.

35. W. Brocks, A. Cornec, and I. Scheider.
Numerical and Computational Methods.
In I. Milne, R. O. Ritchie, and B. Karihaloo, editors, *Compr. Struct. Integr.*, pages 127–209.
Elsevier, 2003.

36. I. Scheider and W. Brocks.
The Effect of the Traction Separation Law on the Results of Cohesive Zone Crack Propagation
Analysese.
Key Eng. Mater., 251-252:313–318, 2003.
doi: 10.4028/www.scientific.net/KEM.251-252.313.

37. V. Tvergaard and J. W. Hutchinson.
The relation between crack growth resistance and fracture process parameters in elastic-
plastic solids.
J. Mech. Phys. Solids, 40(6):1377–1397, 1992.
doi: 10.1016/0022-5096(92)90020-3.

38. Y. F. Gao and A. F. Bower.
A simple technique for avoiding convergence problems in finite element simulations of crack
nucleation and growth on cohesive interfaces.
Model. Simul. Mater. Sci. Eng., 12:453–463, 2004.
doi: 10.1088/0965-0393/12/3/007.

39. H. Yu, J. S. Olsen, V. Olden, A. Alvaro, J. He, and Z. Zhang.
Viscous regularization for cohesive zone modeling under constant displacement: An
application to hydrogen embrittlement simulation.
Eng. Fract. Mech., 166:23–42, 2016.
doi: 10.1016/j.engfracmech.2016.08.019.

40. V. Olden, C. Thaulow, R. Johnsen, and E. Østby.
Cohesive zone modeling of hydrogen-induced stress cracking in 25% Cr duplex stainless steel.
Scr. Mater., 57(7):615–618, 2007.
doi: 10.1016/j.scriptamat.2007.06.006.

41. I. Scheider, M. Pfuff, and W. Dietzel.
Simulation of hydrogen assisted stress corrosion cracking using the cohesive model.
Eng. Fract. Mech., 75(15):4283–4291, 2008.
doi: 10.1016/j.engfracmech.2007.10.002.

42. N. R. Raykar, S. K. Maiti, R. K. Singh Raman, and Saurav Aryan.
Study of hydrogen concentration dependent growth of external annular crack in round tensile
specimen using cohesive zone model.
Eng. Fract. Mech., 106:49–66, 2013.
doi: 10.1016/j.engfracmech.2013.04.007.

43. O. Barrera and A.C.F. Cocks.
Computational modelling of hydrogen embrittlement in welded structures.
Philos. Mag., 93(20):2680–2700, 2013.
doi: 10.1080/14786435.2013.785638.

44. R. A. Oriani and P. H. Josephic.
Equilibrium aspects of hydrogen-induced cracking of steels.
Acta Metall., 22(9):1065–1074, 1974.
doi: 10.1016/0001-6160(74)90061-3.

45. A. Van der Ven and G. Ceder.
The thermodynamics of decohesion.
Acta Mater., 52:1223–1235, 2004.

doi: 10.1016/j.actamat.2003.11.007.

46. D. E. Jiang and E. A. Carter.
First principles assessment of ideal fracture energies of materials with mobile impurities: implications for hydrogen embrittlement of metals.
Acta Mater., 52:4801–4807, 2004.
doi: 10.1016/j.actamat.2004.06.037.

47. E. D. Hondros and M. P. Seah.
The theory of grain boundary segregation in terms of surface adsorption analogues.
Metall. Trans. A, 8(9):1363–1371, 1977.
doi: 10.1007/BF02642850.

48. O. Nguyen and M. Ortiz.
Coarse-graining and renormalization of atomistic binding relations and universal macroscopic cohesive behavior.
J. Mech. Phys. Solids, 50(8):1727–1741, 2002.
doi: 10.1016/S0022-5096(01)00133-8.

49. R. L. Hayes, M. Ortiz, and E. A. Carter.
Universal binding-energy relation for crystals that accounts for surface relaxation.
Phys. Rev. B, 69(17):172104, 2004.
doi: 10.1103/PhysRevB.69.172104.

50. J. P. Hirth.
Effects of hydrogen on the properties of iron and steel.
Metall. Trans. A, 11(6):861–890, 1980.
doi: 10.1007/BF02654700.

51. G. Gobbi, C. Colombo, S. Miccoli, and L. Vergani.
A Numerical Model to Study the Hydrogen Embrittlement Effect.
Procedia Eng., 74:460–463, 2014.
doi: 10.1016/j.proeng.2014.06.297.

52. J. R. Rice and J.-S Wang.
Embrittlement of interfaces by solute segregation.
Mater. Sci. Eng. A, 107:23–40, 1989.
doi: 10.1016/0921-5093(89)90372-9.

53. J.-S. Wang.
The thermodynamics aspects of hydrogen induced embrittlement.
Eng. Fract. Mech., 68(6):647–669, 2001.
doi: 10.1016/S0013-7944(00)00120-X.

54. R. Falkenberg, W. Brocks, W. Dietzel, and I. Scheider.
Modelling the effect of hydrogen on ductile tearing resistance of steel.
Int. J. Mater. Res., 101(8):989–996, 2010.
doi: 10.3139/146.110368.

55. A. Alvaro, V. Olden, and O. M. Akselsen.
3D cohesive modelling of hydrogen embrittlement in the heat affected zone of an X70 pipeline steel.
Int. J. Hydrogen Energy, 38(18):7539–7549, 2013.
doi: 10.1016/j.ijhydene.2013.02.146.